Journal of Luminescence 178 (2016) 368–374

Contents lists available at ScienceDirect

Journal of Luminescence

journal homepage: www.elsevier.com/locate/jlumin

Full Length Article

Structures, and luminescence and magnetic properties of Ln(III) complexes bearing dibenzoylmethane ligand (Ln=Eu and Gd)

Jung-Soo Kang [a,1], Yong-Kwang Jeong [b,1], Yong Suk Shim [c], S. Rout [a], K.T. Leung [a], Youngku Sohn [d,*], Jun-Gill Kang [b,e,**]

[a] WATLab and Department of Chemistry, University of Waterloo, Waterloo, Ontario, Canada, N2L 3G1
[b] Department of Chemistry, Chungnam National University, Daejeon 34134, Republic of Korea
[c] Center for Research Facilities, Chungnam National University, Daejeon 34134, Republic of Korea
[d] Department of Chemistry, Yeungnam University, Gyeongsan, Gyeongbuk 712-749, Republic of Korea
[e] ReSEAT Program, Korea Institute Science and Technology Information, Daejeon 34141, Republic of Korea

ARTICLE INFO

Article history:
Received 4 August 2015
Received in revised form
2 June 2016
Accepted 2 June 2016
Available online 16 June 2016

Keywords:
Ln(III) complex
X-ray crystallography
Sensitized luminescence
Quantum yield
Magnetic susceptibility

ABSTRACT

The single crystal structure, luminescence and magnetic susceptibility of Cs[Ln(DBM)$_4$] and Ln(DBM)$_3$(phen) (Ln=Eu and Gd, DBM=dimenzoylmethanto and phen=1,10-phenanthroine) were characterized in detail. A pentanuclear Eu(III) cluster with the formula, $Eu_5(DBM)_{10}(OH)_5$, was obtained from Cs[Eu(DBM)$_4$] in ethanol, while from Cs[Gd(DBM)$_4$] in acetonitrile, a one-dimensional polymeric Gd(III) assembly with the formula, $\{Cs[Gd(DBM)_4]\}_n$, was achieved via a heterobimetallic backbone, composed of alternating Cs and Gd atoms bridged by DBM. Exciting the Eu(III) complexes with near-UV light produced sensitized red emission by energy transfer from the triplet excited state of DBM to the Eu(III) ion. Replacing DBM by phen increased the quantum yield from $Q=8.3\%$ for Cs[Eu(DBM)$_4$] to $Q=16.6\%$ for Eu(DBM)$_3$(phen). This was attributed to a reduction in the site-symmetry of Eu(III) from D_{4h} to C_{2v}. The magnetic susceptibilities of the synthesized Ln(III) complexes in the crystalline or powder states were measured using a SQUID magnetometer. The Eu(III) complexes illustrated magnetic anisotropy at low temperatures and temperature-dependent susceptibilities. The coercive field inducing the magnetic anisotropy of $Eu_5(DBM)_{10}(OH)_5$ was more than 40-fold stronger than those of Cs[Eu(DBM)$_4$] and Eu(DBM)$_3$(phen). In particular, the calculation based on the Van Vleck's treatment confirmed that the thermal mixing between the excited and ground states played a key role in the temperature-dependent susceptibilities of Eu(III). The magnetic susceptibility of the Gd(III) ion in Gd(DBM)$_3$(phen) was identical to that of the free Gd(III) ion, wheras that of the Gd(III) ion in Cs[Eu(DBM)$_4$] was higher. The phen ligand with the π-conjugate rigid planar structure decreased the magnetic susceptibilities of the Eu(III) and Gd(III) ions.

1. Introduction

Trivalent rare earth ions, Eu(III) and Tb(III), produce red and green luminescence, respectively, when excited with ultraviolet light. However, the intensity is very weak due to their low absorption-cross section in the f→f transitions. To overcome this optical obstacle, an organic ligand is introduced in the complex system as a sensitizer. The chelating ligands strongly absorb UV light and transfers most of the absorbed energy to the rare earth ion, resulting in enhanced luminescence. The typical ligands used as sensitizers include chromophore-functionalized β-diketones. Recently, the sensitized luminescence of β-dikentone-based Ln(III) complexes have been investigated intensively for their applications in light-emitting devices [1–5], as well as in sensors in environmental and biological systems [6–10]. Most β-dikentone-based mononuclear Ln(III) complexes focused on the tris(β-diketonate) formula, Ln(β-diketonate)$_3$, and the ternary mixed-ligand formula, Ln(β-diketonate)$_3$(L), using a bidentate neutral ligand, such as 1,10-phenanthroline (phen) and 2,2′-bipyridine [11]. Previously, a tetrakis(dibenzylmethanto) Eu(III) complex, $[Eu(DBM)_4]^-$, was synthesized to generate strong luminescence, because solvent binding was prevented [12]. For Eu(DBM)$_3$phen, the two different DBM and phen chromophores may complicate the energy transfer process. This study investigated which chromophore was more effective in the sensitized

* Corresponding author. Tel: +82 53 810 2353; fax: +82 53 810 4613.
** Corresponding author at: Department of Chemistry, Chungnam National University, Daejeon 34134, Republic of Korea. Tel: +82 42 821 6548; fax: +82 42 821 8896.
E-mail addresses: youngkusohn@ynu.ac.kr (Y. Sohn), jgkang@cnu.ac.kr (J.-G. Kang).
[1] These authors contributed equally.

http://dx.doi.org/10.1016/j.jlumin.2016.06.008
0022-2313/

luminescence of Eu(III) by characterizing its optical properties. Moreover, the structural and luminescent properties of $[Gd(DBM)_4]^+$ and $Gd(DBM)_3(phen)$ were investigated. The optical properties of the chromophore to the rare earth ion may be different from those of the free chromophore because the paramagnetic metal ion increases the intersystem crossing of the chelating chromophore, resulting in a reduction of the fluorescence intensity and a subsequent increase in the phosphorescence intensity. Generally the observed luminescence of the Gd(III) complex originates from the chromophore because the first excited $^6P_{7/2}$ state of Gd(III) (32,200 cm^{-1}) is higher than the $^1\pi\pi^*$ state of the chromophore [13,14].

Moreover, some Ln(III) ions have high electron spins and large 4f orbital moments, resulting in distinctive magnetic properties [15]. Cui et al. examined the magnetic susceptibility of six $[Ln(NO_3)_x]^{3-x}$ complexes as a function of temperature [16]. Although Ln(III) ions were under an isostructural crystal-field, inconsistent relationships were observed between the observed magnetic properties in the series of Ln(III) ions. Manna et al. also measured the temperature dependence of the magnetic susceptibility of six binuclear Ln(III) complexes with dicarboxylate [17,18]. Antiferromagnetic interactions occurred between two adjacent Ln(III) ions with four Ln(III) ions. Although Gd(III) does not have orbital angular momentum, the Gd(III) complex exhibited super-exchange ferromagnetic properties. In particular, weak antiferromagnetic coupling between the Gd(III) ions was observed in the Ln-organic framework [18]. Therefore, the magnetic properties of Ln(III) complexes are difficult to predict, because they are quite sensitive to the ligand environment. In particular, the unquenched orbital moment of Eu(III) with the $^7F_0$ ground state can give rise to fascinating magnetic properties associated with its anisotropy. Therefore, Ln(III) complexes may be applicable to the in vivo contrast imaging and luminescent probes [19–24]. To date, the magnetic properties of the Ln(III) complexes with homoleptic DBM, and mixed DBM and phen have not been reported. This paper provides details of the crystal structure, sensitizing process, and magnetic susceptibility of $Eu_5(DBM)_{10}(OH)_5$, $[Ln(DBM)_4]^-$ and $Ln(DBM)_3(phen)$ (Ln=Eu and Gd).

2. Experimental section

2.1. Synthesis and composition analysis

$EuCl_3 \cdot 6H_2O$ (99%), $GdCl_3 \cdot 6H_2O$ (99%), dibenzoylmethane (DBMH) (99%), and 1,10-phenanthroline (99%) were purchased from Aldrich. The organic solvents were obtained from Samchun. All chemicals were used without further purification.

Elementary analysis (EA) of the carbon, hydrogen and nitrogen contents was performed using a CE EA-1110 elemental analyzer. The cations were analyzed quantitatively with an Optima 7100 inductively coupled plasma (ICP) atomic emission spectrometer.

Complexes of $Cs[Ln(DBM)_4]$ (Ln=Ed and Gd) were synthesized using a method described elsewhere [12]. For $[Ln(DBM)_3(phen)]$ (Ln=Ed and Gd), 3 mmol of DBMH in 5 mL of ethanol was added to a solution of 1 mmol of $LnCl_3 \cdot 6H_2O$ and 1 mmol of phen in a 1:1 water-ethanol mixed solvent (20 mL). After adjusting the pH of the solution between 7–7.5 with dilute CsOH solution, the resulting solution was stirred for 2 h at room temperature. After filtering and washing several times with water and ethanol, alternately, the precipitate was dried in an electric oven.

Anal. Calcd. for $Cs[Gd(DBM)_4]$: Cs 11.2; Gd 13.2; C 60.9; H 3.8%. Found: Cs 10.4; Gd 13.3; C 60.2; H 3.8%. IR data (cm^{-1}): 1597, 1529, 1471, 1405, 1375, 1311, 1068, 1019, 755, 689, 621, 532.

Anal. Calcd. for $[Eu(DBM)_3(phen)]$: Eu 15.1; C 68.1; H 4.4; N 2.8%. Found: Eu 16.6; C 68.5; H 4.2; N 2.7%. IR data (cm^{-1}): 1596, 1550, 1519, 1477, 1411, 1305, 1283, 1219, 1066, 1024, 841, 748, 723, 688, 608, 511.

Anal. Calcd. for $[Gd(DBM)_3(phen)]$: Gd 15.6; C 68.0; H 3.8; N 2.8%. Found: Gd 16.0; C 68.3; H 4.1; N 2.7%. IR data (cm^{-1}): 1599, 1552, 1517, 1467, 1409, 1302, 1219, 1068, 1026, 847, 726, 611, 517.

With the exception of $Cs[Eu(DBM)_4]$, suitable single crystals of the prepared complexes, $Cs[Gd(DBM)_4]$ and $[Ln(DBM)_3(phen)]$ (Ln=Eu and Gd), were grown from an acetonitrile solution by a slow-evaporation method. Determination of the unit cell constants of the obtained single crystals via single crystal X-ray diffraction confirmed the desired formation of the $Cs[Gd(DBM)_4]$ and $[Ln(DBM)_3(phen)]$ (Ln=Eu and Gd) complexes. For $Cs[Eu(DBM)_4]$, the single crystals were obtained from an ethanol solution. Anal. Calcd. for $Eu_5(DBM)_{10} \cdot (OH)_5$, cal.: Eu 24.7, C 58.5, H 3.8%. Found: Eu 23.5, C 60.1, H 3.7%. IR (cm^{-1}): 1595, 1557, 1478, 1408, 1310, 1229, 1061, 1026, 835, 756, 704, 683, 611.

2.2. X-ray crystallography

The diffraction data were collected on a Bruker Smart CCD diffractometer using graphite monochromated MoKα-radiation (λ=0.71073 Å) at room temperature. The structure was solved by applying the direct method and refined by a full-matrix least-squares calculation on F^2 using SHELXL [25]. All hydrogen atoms were calculated in the ideal positions and attached to the appropriate carbon atom. The crystal data and refinement results are summarized in Table S1 (Supplementary material).

2.3. Spectroscopic and magnetic measurements

The luminescence and excitation spectra, and the luminescence lifetime were measured using previously described methods [12]. The magnetic studies were performed on polycrystalline or powder samples using a MPMS SQUID magnetometer (Quantum Design, USA). The zero-field cooled (ZFC) and the field-cooled (FC) magnetization measurements were taken upon warming after zero-field cooling and subsequent cooling over the temperature range, 5–300 K, in an applied field of 1000 Oe. The field dependence of the magnetization was also measured at T=2, 5, 77, and 300 K. Pascal's constants were used to estimate the diamagnetic correction ($\chi_{M,D}$), which was subtracted from the experimental molar susceptibility ($\chi_{M,exp}$) to give the molar paramagnetic susceptibility [26].

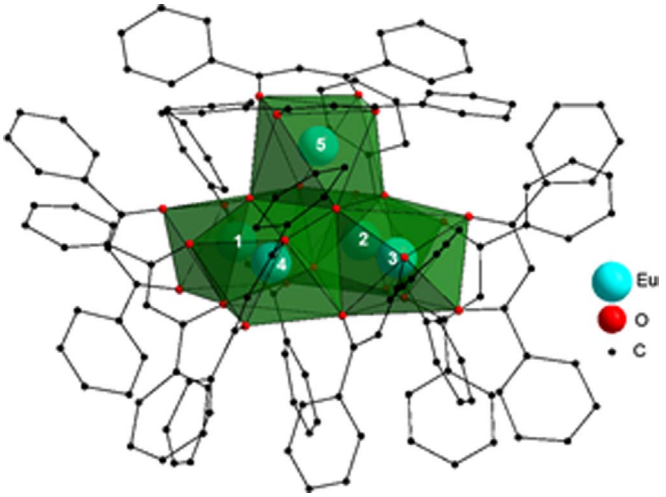

Fig. 1. Prospective view of $Eu_5(\mu_4\text{-}OH)(\mu_3\text{-}OH)_4(\mu\text{-}DBM)_4(DBM)_6$. Hydrogen atoms are omitted for clarity.

$$5Cs[Ed(DBM)_4] + 10C_2H_5OH \xrightarrow[-5[DBMH + \{C_6H_5C(O)\}_2CHC_2H_5]]{-5C_2H_5OCs} Eu_5(OH)_5(DBM)_{10}$$

Scheme 1. Reaction scheme for the pentanuclear Eu(III) complex.

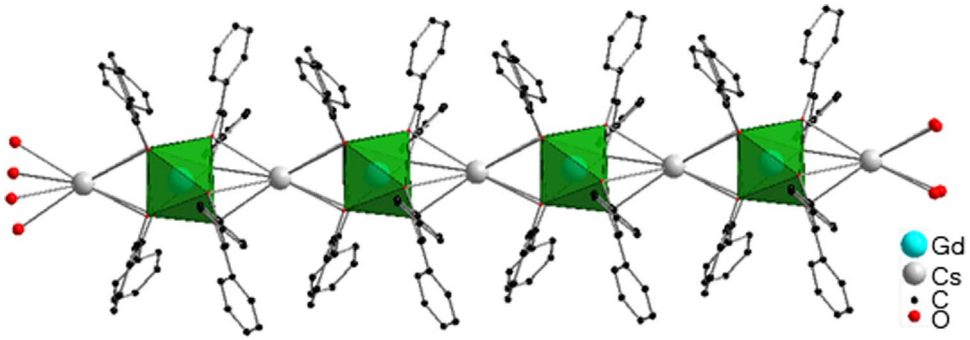

Fig. 2. Polymeric assembly of $Cs[Gd(DBM)_4]$. Hydrogen atoms are omitted for clarity.

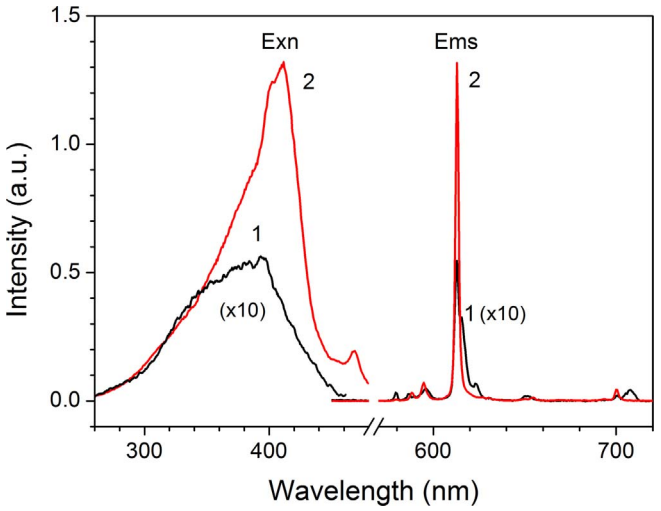

Fig. 3. Emission (λ_{exn}=398 nm) and excitation (λ_{ems}=612.8 nm) spectra of $[Eu_5(DBM)_{10}(OH)_5]$ (1) in the crystalline state and $Cs[Eu(DBM)_4]$ (2) in the powdered state at RT.

3. Results and discussion

3.1. Crystal structure

The $Eu_5(DBM)_{10}(OH)_5$ complex crystallized in the monoclinic space $P2_1/c$. As shown in Fig. 1, the single crystals, which were grown from an ethanol solution of tetrakis(dibenzylmethanto) Eu(III), formed a pentanuclear Eu_5 polyhedron with the formula, $Eu_5(\mu_4\text{-OH})(\mu_3\text{-OH})_4(\mu\text{-DBM})_4(DBM)_6$. Previously, the pentanuclear Ln_5 complexes were obtained by a reaction in the presence of N-methylmorpholine [27] or triethylamine [28–30]. On the other hand, in the absence of amines or catalysts, the cesium ion could play a key role in the deprotonation of ethanol, resulting in the decomposition of DBM (Scheme 1). Table S2 lists the selected bond lengths and angles. As shown in Fig. 1, each Eu atom was coordinated to eight oxygen atoms, adopting a square antiprism geometry.

The $Cs[Gd(DBM)_4]$ complex crystallized in the monoclinic space group, C2/c, and the complete molecule was generated by the site symmetry of a crystallographic two-fold rotation axis. As shown in Fig. 2, the complex formed a one-dimensional supramolecular polymer in the crystalline state, which was composed of alternating Gd and Cs that were bridged by the DBM ligands. Gd atoms also achieve 8-coordination by the eight oxygen atoms from the four DBM ligands. As listed in Table S3, the Gd–O bond distances ranged from 2.340(19) to 2.409(2) Å. These distances were more than 0.10 Å longer than Ln–O in $Ln(DBM)_3 \cdot H_2O$ (Ln=Ho and Yb) [31,32].

For $[Ln(DBM)_3(phen)]$ (Ln=Eu and Gd), the complexes crystallized in the monoclinic space group $P2_1/c$ and the triclinic space group P-1, respectively. Fig. S1 shows a perspective view of the Eu(III) crystalline form. Tables S4 and S5 list the selected bond lengths and angles of the two complexes. The central Ln(III) ion is coordinated by six oxygen atoms from three DBM ligands and two nitrogen atoms from phen. The bond lengths and bond angles formed by the central Ln atom are comparable to those reported elsewhere [32]. Eight-coordinated polyhedrons most frequently form dodecahedrons or square antiprisms [33]. The square antiprism geometry can be accessed by the two rectangular and six triangular faces. The calculated locations of the N and O atoms were displaced from their mean planes by less than $\pm$0.04 Å for the Eu(III) crystals and $\pm$0.10 Å for the Gd(III) crystals. The displacement of each atom from the mean plane indicates that the Ln(III) complex forms a slightly distorted square antiprism polyhedron.

3.2. Sensitized luminescence and quantum yield

3.2.1. Luminescence and excitation spectra

The absorption spectra of the free ligands, DBMH and phen, and two Eu(III) complexes were measured in a methanol solution. As shown in Fig. S2, the DBM ligand and $[Eu(DBM)_4]^+$ complex produced two apparent absorption bands at ~350 nm as the main peak and ~250 nm as the minor (hereafter referred to as A- and B-bands, respectively, in order of increasing energy). Table S6 lists the resolution of the electronic absorption band using a Gaussian formula. A comparison of the peak positions and the relative intensities of the observed bands between the complex and ligands confirmed that the A-band and C-band (λ_{max}=227 nm) of the complex were assigned to the $\pi \rightarrow \pi^*$ transitions of DBM and phen, respectively, and the B-band was a combination of the B-band of DBM and the A-band of phen.

Fig. 3 shows the emission and excitation spectra of $Eu_5(DBM)_{10}(OH)_5$ in the crystalline state and $Cs[Eu(DBM)_4]$ in the powdered state, which were measured at room temperature. When excited at 398 nm, both produced typical luminescence features in the 570–720 nm region, arising from the $^5D_0 \rightarrow {}^7F_J$ (J=0–4) transitions of Eu(III). A very strong and narrow luminescence band at 612.8 nm, which was labeled as hypersensitive, resulted from the $^5D_0 \rightarrow {}^7F_2$ transition of Eu(III).

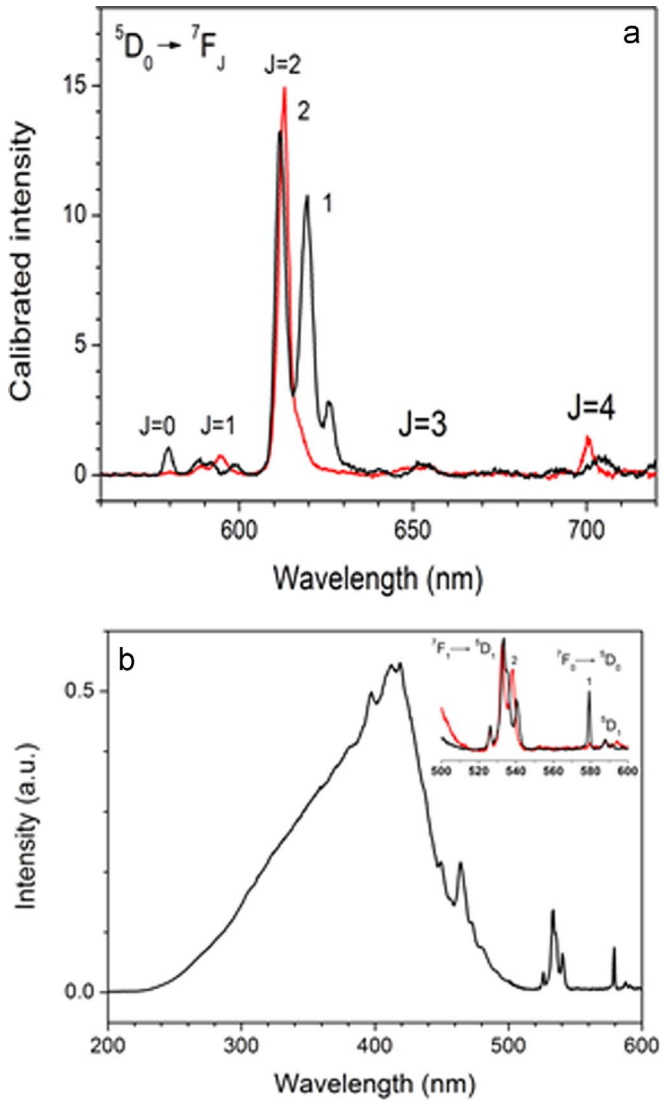

Fig. 4. (a) Calibrated emission spectra of $Eu(DBM)_3(phen)$ (1) and $Cs[Eu(DBM)_4]$ (2) (λ_{exn}=405 nm), and (b) excitation spectrum of $Eu(DBM)_3(phen)$ (λ_{ems}=612 nm) measured at room temperature.

Significant spectral differences in this hypersensitive band between the two complexes can be found in the intensity and band structure. For $[Eu(DBM)_4]^-$, the band shape was a singlet and its intensity was more than 20 times stronger than that of $Eu_5(DBM)_{10}(OH)_5$ with a triplet band-shape, peaking at 612.8 (vs), 615.5 (s) and 623.0 (vw) nm. The band structure shows that the extent to which the $(2J+1)$ degeneracy of $^7F_2$ is removed depends on the site symmetry. As observed from the crystal structures, each of the Eu atoms in $Eu_5(DBM)_{10}(OH)_5$ is surrounded by a different set of oxygen atoms, whereas the Eu atom in $[Eu(DBM)_4]^-$ was surrounded by eight equivalent oxygen atoms. For the $Eu_5(DBM)_{10}(OH)_5$ complex, the OH groups bonded to Eu(III) caused a significant decrease in luminescence intensity. The excitation spectrum of $[Eu(DBM)_4]^-$ was more characteristic than that of $Eu_5(DBM)_{10}(OH)_5$, because of its stronger emission intensity. For $[Eu(DBM)_4]^-$ and $Eu_5(DBM)_{10}(OH)_5$, however, the broad band, peaking at 420 nm and 400 nm, respectively, correspond to the A-absorption band of each complex. The spectral characteristics showed that the red emission from Eu(III) was generated by energy transfer from the DBM ligand.

The emission and excitation spectra of the $Eu(DBM)_3(phen)$ complex were also measured and compared with those of $[Eu(DBM)_4]^-$, as shown in Fig. 4. For $Eu(DBM)_3(phen)$, the effect of the site symmetry of Eu(III) on the band structure was more obvious, compared to $[Eu(DBM)_4]^-$. For the hypersensitive emission, the $Eu(DBM)_3(phen)$ complex produced three lines, whereas the $[Eu(DBM)_4]^-$ complex produced only a single line. Assuming that $[Eu(DBM)_4]^-$ is isostructural with $[Gd(DBM)_4]^-$, the site symmetry of Eu in $[Eu(DBM)_4]^-$ surrounded by eight equivalent O atoms is D_{4h}, and that of Eu in $Eu(DBM)_3(phen)$ surrounded by two N and six O atoms is C_{2v}, (Figs. 2 and S1). Taking into account selection rules for the $^5D_0 \rightarrow {}^7F_J$ (J=0–4) transitions of Eu(III) in the D_{4h} and C_{2v} symmetries (Table S7), the number of lines observed in the hypersensitive band well reflects the effects of the site symmetry of Eu(III) on the band structure. Unlike other $^5D_0 \rightarrow {}^7F_J$ transitions, the $^5D_0 \rightarrow {}^7F_1$ transition for most of Eu(III) complexes is allowed by the magnetic dipole moment. Therefore, this transition well reflects the site symmetry of the Eu(III) ion in the number of lines and its intensity is almost independent of the environment with moderate intensity, as shown in Fig. 4(a): two lines for $[Eu(DBM)_4]^-$ and three lines for $Eu(DBM)_3(phen)$. The excitation spectrum of the 611.5-nm emission from $Eu(DBM)_3(phen)$ complex was similar to that of $[Eu(DBM)_4]^-$. A series of weak bands at 394, 465 and 526 nm, corresponding to the Eu(III) direct transitions, was superimposed on the broad band. Additional excitation bands, which appeared in the 500–600 nm range (inserted in Fig. 4(b)), corresponded to the transitions from the $^7F_1$ and $^7F_0$ states to the $^5D_1$ state. The broad band, peaking at 405 nm, was the result of energy transfer from DBM to Eu(III). For $Eu(DBM)_3$(5-amino-phen) covalently assembled on a functionalized silica surface, the relative emission intensity between the $^5D_0 \rightarrow {}^7F_1$ and $^5D_0 \rightarrow {}^7F_2$ transitions was found to vary upon the excitation wavelength of the energy transfer band [34,35]. For most of europium complexes with phen the energy transfer from phen to Eu(III) appeared in the 250–380 nm excitation region. These results suggest that the excitation process via DBM was more effective than that via phen. Any optical processes of phen in the complex are suppressed entirely by DBM within $Eu(DBM)_3(phen)$. This could be because the energy gap between the $^3\pi\pi^*$ donating level of DBM and the emitting $^5D_0$ level of Eu(III) is smaller than the case resulting from phen: ΔE_{gap}=7450 cm^{-1} for DBM and ΔE_{gap}=11170 cm^{-1} for phen. The PL and excitation spectra of $[Gd(DBM)_4]^-$ and $Gd(DBM)_3(phen)$ were also measured to assess the role of the two chromophores in the sensitized luminescence of Eu(III) in $Eu(DBM)_3(phen)$. The spectral features of the PL and the excitation of $Gd(DBM)_3(phen)$ are similar to those of $[Gd(DBM)_4]^-$. The 325-nm excitation produced bell-type emission from both, peaking at 502 nm, and its excitation peaked at 405 nm (Fig. S3). The spectra were resolved to three Gaussian components, peaking at 440, 489 and 542 nm. Taking the mirror image and the Stokes shift into consideration, the first two components can be assigned to fluorescence and the low-energy component can be assigned to phosphorescence. Note that the luminescence peaking at 410 nm was produced from $[Gd(phen)_2]^{3+}$ by the 325-nm excitation. The excitation spectra of the 570-nm emission from $Gd(DBM)_3(phen)$ and $[Gd(DBM)_4]^-$ were similar to the energy-transfer band of Eu $(DBM)_3(phen)$.

Table 1
Sensitized-luminescence quantum yield (Q) and decay time (τ) of $Cs[Eu(DBM)_4]$ and $Eu(DBM)_3(phen)$ in powder.

Sample	τ (ms)[a]	Q_{sen}[b]	Q_{Eu}^{Eu}	η_{ET}^{L}
$Cs[Eu(DBM)_4]$	0.36	0.083	0.29	0.29
$Eu(DBM)_3(phen)$	0.25	0.17	0.31	0.54

[a] Excitation: 337 nm.
[b] Excitation: 405 nm.

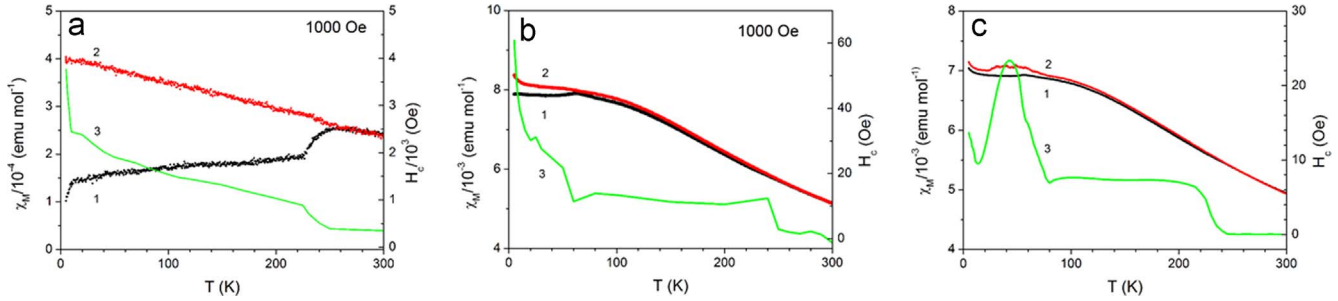

Fig. 5. Temperature dependence of molar susceptibilities of $[Eu_5(DBM)_{10}\cdot(OH)_5]$ (a) in the crystalline state, $Cs[Eu(DBM)_4]$ (b), $Eu(DBM)_3(phen)$ (c) via ZFC (1) and FC (2) magnetizations, and coercivity field (H_c, 3) calculated from $\chi_{M,ZFC}$ and $\chi_{M,FC}$.

Table 2
Molar magnetic subsceptibilities and effective Bohr magneton numbers of Eu(III) complexes.

Complex	χ_M (10^{-4} emu mol^{-1})			μ_{eff} (10^{-21} emu)		
	5 K	77 K	300 K	5 K	77 K	300 K
$Eu_5(DBM)_{10}\cdot(OH)_5$	4.03	3.63	2.34	2.38	2.26	2.08
$Cs[Eu(DBM)_4]$	8.37	7.91	5.13	10.9	10.5	9.74
$Eu(DBM)_3(phen)$	6.61	6.40	4.41	9.65	9.48	9.03

3.2.2. Quantum yield

The luminescence lifetime and the absolute sensitized-luminescence quantum yield of the Eu(III) complexes prepared in powder were determined precisely at room temperature. As listed in Table 1, no significant difference in the lifetime was observed between the two complexes, while the quantum yield of $Eu(DBM)_3(phen)$ ($Q_{sen}=0.17$) was 2 times larger than that of $Cs[Eu(DBM)_4]$ ($Q_{sen}=0.083$). Note that the absorption coefficients of $Cs[Eu(DBM)_4]$ and $Eu(DBM)_3(phen)$ were calculated to be 0.96 and 0.79, respectively. The observed quantum yield of the sensitized luminescence of the Eu(III) complexes, Q_{sen}, is associated with the efficiency of the energy transfer from the ligand to europium (η_{ET}^{L}), and radiative and nonradiative processes (Q_{Eu}^{Eu}), occurring from the receiving levels to the $^7F_0$ ground state as $Q_{sen}=\eta_{ET}^{L}\times Q_{Eu}^{Eu}$. The term of Q_{Eu}^{Eu} has been estimated using the observed luminescence lifetime, τ_{obs}, and the natural lifetime, τ_o, using $Q_{Eu}^{Eu}=\tau_{obs}/\tau_o$. The natural lifetime, which is responsible for the $^5D_0\rightarrow{}^7F_0$ transition, could not be measured directly because of its faint or forbidden intensities. Wertset et al. reported the estimation of τ_o from the shape of the corrected emission spectrum, using the formula [36].

$$\frac{1}{\tau_0}=A_{MD,0}n^3\left(\frac{I_{tot}}{I_{MD}}\right)$$

where the MD-allowed probability of the $^5D_0\rightarrow{}^7F_0$ transition, $A_{MD,0}$, is a constant as 14.65 s^{-1} and the refractive index, n, was assumed to 1.5 for a solid sample. The term, (I_{tot}/I_{MD}), was the ratio of the total area of the observed emission. Using these approximations, Q_{Eu}^{Eu} and η_{ET}^{L} were calculated for the two Eu(III) complexes. As listed in Table 1, the energy-transfer efficiency from DBM to Eu(III) in $Eu(DBM)_3(phen)$ was ~ two times larger than that in $Cs[Eu(DBM)_4]$. This shows that the site symmetry of Eu(III) plays a key role in determining the luminescence efficiency, particullary depending on the extent to which the $(2J+1)$ degeneracy of $^7F_2$ is removed. For Eu (III) in the $Cs[Eu(DBM)_4]$ complex, the hypersensitive band consists of only a single transition from the A_{1g} level to the E_g level, whereas for the $Eu(DBM)_3(phen)$ complex, the hypersensitive band consists of the three transitions from the A_1 level ($^5D_0$) to the A_2, B_1, and B_2 levels ($^7F_2$).

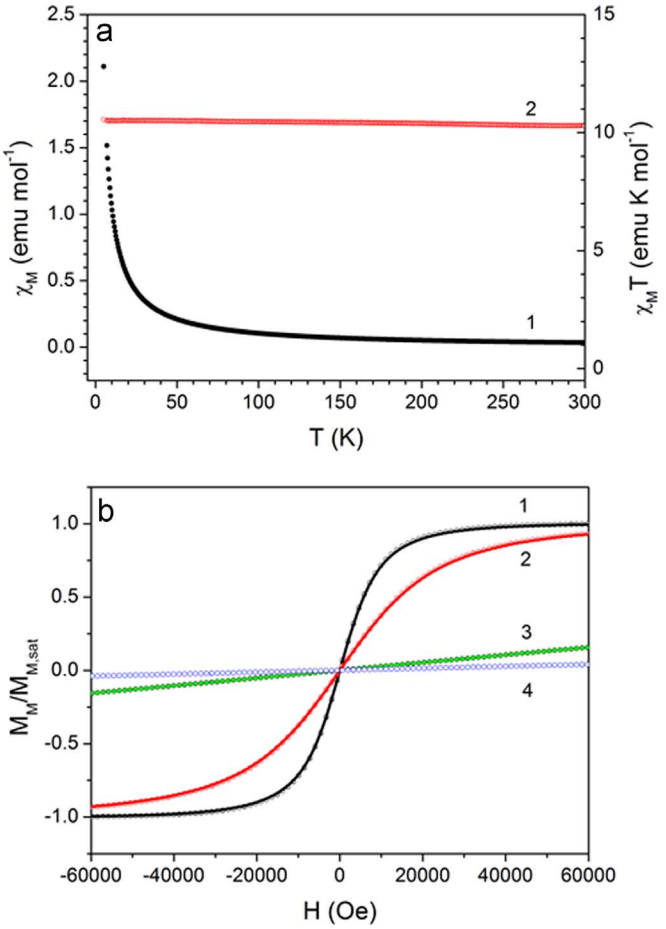

Fig. 6. (a) Temperature dependences of χ_M (1) and $\chi_M T$ (2), and (b) field dependence of $M_M/M_{M,sat}$ of $Cs[Gd(DBM)_4]$ at T=1; 2 K, 2; 5 K, 3; 77 K, 4; 300 K. The solid lines (1, 2) at T=2 and 5 K represent the fitted values using the Brillouin function.

3.3. Magnetic properties

3.3.1. Eu(III) complex

The ZFC and FC molar susceptibilities of the three Eu(III) complexes were measured over the temperature range of 5–300 K. For $Eu_5(DBM)_{10}\cdot(OH)_5$, the temperature dependence of $\chi_{M,ZFC}$ was anomalous (Fig. 5(a)). Four distinctive steps were observed in the temperature ranges, 5–11 K, 11–225 K, 225–259 K, and 259–300 K. At T=5 K, $\chi_{M,ZFC}$ was 1.90×10^{-4} emu mol^{-1}. With increasing temperature, $\chi_{M,ZFC}$ increased, rapidly in the first step and gradually in the second step. In the third step, the increase in $\chi_{M,ZFC}$ escalated but slowed down gradually. At T=257 K, $\chi_{M,ZFC}$ reached a maximum (3.47 emu mol^{-1}), corresponding to the block temperature (T_B). Above this temperature, $\chi_{M,ZFC}$ decreased gradually with increasing

temperature. Upon subsequent cooling from 300 to 259 K, the $\chi_{M,FC}$ values were identical to those of $\chi_{M,ZFC}$. Below $T=259$ K, $\chi_{M,FC}$ increased gradually with decreasing temperature and showed irreversibility with regard to $\chi_{M,ZFC}$. The difference between $\chi_{M,ZFC}$ and $\chi_{M,FC}$ below T_B resulted mainly from the existence of energy barriers of magnetic anisotropy. During the ZFC process, the spins were locked in random directions for the Eu(III) complexes. At $T=5$ K, the applied magnetic field ($H_{app}=1000$ Oe) was insufficient to rotate the spins in the direction of the applied field, resulting in low susceptibility. The observed $\chi_{M,ZFC}$ reflected only the contribution of the particles that overcame the energy barriers specified as the coercive field strength, H_c. Using the relationship between $\chi_{M,FC}$ and $\chi_{M,ZFC}$ (Eqs. (S1) and (S2)) [37], H_c was calculated from the observed ZFC and FC molar susceptibilities. As shown in Fig. 5(a), at $T=5$ K, the coercive field strength reached more than 3500 Oe, which is much stronger than the applied magnetic field. These results showed that the magnetic anisotropy of the Eu(III) ion in $Eu_5(DBM)_{10}\cdot(OH)_5$ was effective in inducing the single-molecule magnet properties below $T=257$ K. In addition, the field dependence of magnetization of $Eu_5(DBM)_{10}\cdot(OH)_5$ was measured at 2, 5, 77, and 300 K. Fig. S4 shows uncorrected molar magnetization of $Eu_5(DBM)_{10}(OH)_5$ measured at $T=2$ K. The negative magnetization was observed for $Eu_5(DBM)_{10}(OH)_5$ at the four temperatures. This might be because in $Eu_5(DBM)_{10}(OH)_5$, the demagnetization of the ligands ($\chi_M=-1.44\times10^{-3}$ emu mol^{-1}) is greater than the magnetization of Eu(III) ($\chi_{M,ZFC}=1.90\times10^{-4}$ emu mol^{-1} at 5 K). For Cs[Eu(DBM)$_4$] and Eu(DBM)$_3$(phen), the magnetic anisotropy in the ZFC and the FC molar susceptibilities were negligible (Fig. 5 (b) and (c)) above $T=80$ K. On the other hand, the calculated H_c values were very low, even at low temperatures (≤ 60 Oe), so that the hysteresis symptom did not appear in the field dependence of molar magnetization even at low temperatures.

For Eu(III) and Sm(III), the energy interval, $\Delta E(J)$, between two consecutive J and $J+1$ states, are not very great compared to kT (0.689 T cm^{-1}). Van Vleck predicted that for Eu(III) and Sm(III), the splitting of the excited states by a surrounding crystal field and the thermal population of the crystal-field levels caused a second-order contribution to the magnetic susceptibility [38]. Using Eq. (S3) with $\mu_B=9.27\times10^{-21}$ emu for the free atom, the molar susceptibility of the three Eu(III) complexes was calculated and compared with the observed $\chi_{M,FC}$ values. As shown in Fig. S5, the values observed for Eu(DBM)$_3$(phen) were quite close to the theoretical values. Those of $Eu_5(DBM)_{10}(OH)_5$, however, were considerably lower than the calculated ones. This suggested that the distortion by interatomic forces in the $Eu_5(DBM)_{10}(OH)_5$ complex could be significant. Therefore, the atomic permanent moment ($\mu_B=9.27\times10^{-21}$ emu) was not valuable for the Eu(III) complex. The phenomenological temperature-dependent effective Bohr magnetic moment was considered to be a second-order correction. By replacing μ_B with μ_{eff} in Eq. (S3), the experimental μ_{eff} was determined by fitting the observed $\chi_{M,FC}$. As listed in Table 2, the experimental μ_{eff} of $Eu_5(DBM)_{10}\cdot(OH)_5$ varied from 2.08×10^{-21} emu (300 K) to 2.38×10^{-21} emu (5 K). These values were less than 1/4, compared to the permanent moment μ_B. For Cs[Eu(DBM)$_4$] and Eu(DBM)$_3$(phen), the experimental μ_{eff} values were close to μ_B. These results showed that the interatomic-force distortion was negligible for these two complexes.

3.3.2. Gd(III) complexes

The ZFC and the FC molar susceptibilities of the Cs[Gd(DBM)$_4$] and Gd(DBM)$_3$(phen) complexes were also measured over the temperature range, 5–300 K. No magnetic anisotropy was observed for the Gd(III) complexes, because $\chi_{M,ZFC}$ and $\chi_{M,FC}$ were identical at a given temperature. As shown in Fig. 6(a), the Cs[Gd(DBM)$_4$] complex is strongly paramagnetic, and χ_MT was temperature-independent. The experimentally determined χ_MT value was 10.42 emu K mol^{-1} ($\sigma=\pm0.07$) over the observed temperature range. According to the free-ion approximation of the Gd(III) ion, the theoretical value of χ_MT for the $^8S_{7/2}$ ($S=7/2$, $L=0$, $J=7/2$) ground state was calculated to be 7.88 emu mol^{-1}. The observed χ_MT value at $H_{ext}=1000$ Oe was slightly higher than the value of the Gd(III) free-ion state. A plot of $1/\chi_M$ versus T obeyed the Curie–Weiss law (Fig. S6). The Curie constant and Weiss temperature were determined to be $C=10.45$ emu K mol^{-1} and $\Theta=0.88$ K, respectively. The magnetic-field dependence of the magnetization of Cs[Gd(DBM)$_4$] were measured at 2, 5, 77 and 300 K. As shown in Fig. 6(b), at $T=2$ K, with increasing magnetic field, the relative molar magnetization, $M_M/M_{M,sat}$, of the Gd(III) complex increased and became saturated at a high field ($M_{M,sat}=52400$ emu). The magnetic-field dependences of the molar magnetization of the Gd(III) complex at $T=2$ and 5 K were fitted using the Brillouin function. The best fitting resulted in $g_{eff}=2$ and $\mu_{eff}=9.27\times10^{-21}$ emu. These values showed that the overall magnetic properties of the Gd(III) ion in the complex were identical to those of the Gd(III) free ion with $g_J=2$. The observed magnetic properties of the Gd(DBM)$_3$(phen) complex are comparable to those of the Cs[Gd(DBM)$_4$] complex (Figs. S7 and S8). The value of χ_MT obtained was 7.41 emu mol^{-1} over the 5–300 K range and the Curie–Weiss fitting resulted in $C=7.44$ emu K mol^{-1} and $\Theta=0.14$ K. The observed χ_MT of the Gd(III) ion in Gd(DBM)$_3$(phen) was slightly lower than that of the free Gd(III) ion. For the magnetization of lanthanide ions the ligand phen with a π-conjugate rigid planar structure could be less effective than DBM with two phenyl terminal groups.

4. Conclusions

An ethanol solution of Cs[Eu(DBM)$_4$] yielded a pentanuclear europium cluster with the composition $Eu_5(\mu_4\text{-}OH)(\mu_3\text{-}OH)_4(\mu\text{-}DBM)_4(DBM)_6$. The cluster produced a hypersensitive red emission via energy transfer from DBM to Eu(III). On the other hand, the emission intensity of the cluster was markedly weaker than those of Cs[Eu(DBM)$_4$] and Eu(DBM)$_3$(phen), because of OH quenching. The DBM ligand played a key role in producing the sensitized luminescence of Eu(III). The energy-transfer route via phen was suppressed entirely by DBM in Eu(DBM)$_3$(phen). An acetonitrile solution of Cs[Gd(DBM)$_4$] yielded a one-dimensional polymeric assembly. The molar susceptibilities of Cs[Gd(DBM)$_4$] were slightly larger than that of Gd(DBM)$_3$(phen). The ligand phen with a π-conjugate planar structure may be less effective than DBM in the magnetization of lanthanide ions.

Acknowledgments

This research was supported by National Research Foundation (2012R1A1A22007201). J.-G.K. and Y.S. acknowledge the ReSEAT program funded by the Ministry of Science, ICT and Future Planning through, the National Research Foundation of Korea and the Korea Lottery Commission grants.

Appendix A. Supplementary material

Supplementary data associated with this article can be found in the online version at http://dx.doi.org/10.1016/j.jlumin.2016.06.008.

References

[1] L.D. Carlos, R.A.S. Ferreira, V. de Zea Bermudez, S.J.L. Ribeiro, Adv. Mater. 21 (2009) 509.
[2] L. Armelao, S. Quici, F. Barigelletti, G. Accorsi, G. Bottaro, M. Cavazzini, E. Tondello, Coord. Chem. Rev. 254 (2010) 487.
[3] Y. Wang, Z. Jiang, Y. Lv, Y. Zhang, D. Ma, F. Zhang, B. Tan, Synth. Met. 161 (2011) 655.

[4] Y. Wang, D. Ma, Z. Jiang, Y.J. Zhang, H. Yuan, Y. Lv, H. Liu, Y. Zhu, W. Fang, Adv. Mater. Res. 512-515 (2012) 1767.
[5] P.P. Lima, F.A.A. Paz, C.D.S. Brites, W.G. Quirino, C. Legnani, M. Costa e Silva, R.A. S. Ferreira, S.A. Junior, O.L. Malta, M. Cremona, L.D. Carlos, Org. Electron. 15 (2014) 798.
[6] T.L. Esplin, M.L. Cable, H.B. Gray, A. Ponce, Inorg. Chem. 49 (2010) 4643.
[7] G. Cui, Z. Ye, R. Zhang, G. Wang, J. Yuan, J. Fluoresc. 22 (2012) 261.
[8] M. Liu, Z. Ye, G. Wang, J. Yuan, Talanta 99 (2012) 951.
[9] M. Schaeferling, T. Aeaeritalo, T. Soukka, Chem. Eur. J. 20 (2014) 5298.
[10] N. Hildebrandt, K.D. Wagner, W.R. Algar, Coord. Chem. Rev. 273-274 (2014) 125.
[11] K. Binnemans, Rare-earth beta-diketonates, in: K.A. Gschneidner, J.-C.G. Bünzli Jr., V.K. Pecharsky (Eds.), Handbook on the Physics and Chemistry of Rare Earths, 35, Elsevier, North Holland, 2005, Chapter 225.
[12] Y.-K. Jeong, Y. Sohn, J.-G. Kang, J. Colloid Interface Sci. 423 (2014) 41.
[13] S. Tobita, M. Arakawa, I. Tanaka, J. Phys. Chem. 88 (1984) 2697.
[14] S. Tobita, M. Arakawa, I. Tanaka, J. Phys. Chem. 89 (1985) 5649.
[15] J. Jensen, A.R. Mackintosh, Rare Earth Magnetism, Clarendon Press, Oxford, 1991.
[16] H. Cui, T. Otsuka, A. Kobayashi, N. Takeda, M. Ishikawa, Y. Misaki, H. Kobayashi, Inorg. Chem. 42 (2003) 6114.
[17] S.C. Manna, E. Zangrando, A. Bencini, C. Benelli, N.R. Chaudhuri, Inorg. Chem. 45 (2006) 9114.
[18] H.-J. Zhang, X.-Z. Wang, D.-R. Zhu, Y. Song, Y. Xu, H. Xu, X. Shen, T. Gao, M.-X. Huang, CrystEngComm 13 (2011) 2586.
[19] J.-M. Jia, S.-J. Liu, Y. Cui, S.-D. Han, T.-L. Hu, X.-H. Bu, Cryst. Growth Des. 13 (2013) 4631.
[20] N. Saini, R. Varshney, A.K. Tiwari, A. Kaul, M. Allard, M.P.S. Ishar, A.K. Mishra, Dalton Trans. 42 (2013) 4994.
[21] M.R. Berwick, D.J. Lewis, A.W. Jones, R.A. Parslow, T.R. Dafforn, H.J. Cooper, J. Wilkie, Z. Pikramenou, M.M. Britton, A.F.A. Peacock, J. Am. Chem. Soc. 136 (2014) 1166.
[22] E. Debroye, S.V. Eliseeva, S. Laurent, E.L. Vander, R.N. Muller, T.N. Parac-Vogt, Dalton Trans. 43 (2014) 3589.
[23] S.S. Kelkar, L. Xue, S.R. Turner, T.M. Reineke, Biomacromolecules 15 (2014) 1612.
[24] S. Laurent, E. Vander, G.C. Luce, N. Leygue, S. Boutry, C. Picard, R.N. Muller, Contrast Media Mol. Imaging 9 (2014) 300.
[25] G.M. Sheldrick, Acta Cryst. C71 (2015) 3.
[26] G.A. Bain, J.F. Berry, J. Chem. Educ. 85 (2008) 532.
[27] R.-E. Xiong, J.-L. Zuo, Z. Yu, X.-Z. You, W. Chen, Inorg. Chem. Commun. 2 (1999) 490.
[28] M.T. Gamer, Y. Lan, P.W. Roesky, A.K. Powell, R. Clérac, Inorg. Chem. 47 (2008) 6581.
[29] P.W. Roesky, G. Canseco-Melchor, A. Zulys, Chem. Commun. (2004) 738.
[30] A.K. Jami, P.V.V.N. Kishore, V. Baskar, Polyhedron 28 (2009) 2284.
[31] A. Zalkin, D.H. Templeton, D.C. Karraker, Inorg. Chem. 8 (1969) 2680.
[32] M.O. Ahmed, J.-L. Liao, X. Chen, S.-A. Chenb, J.H. Kaldis, Acta Cryst. E59 (2003) m29.
[33] J.L. Hoard, J.V. Silverton, Inorg. Chem. 2 (1963) 235.
[34] A. Gulino, F. Lupo, G.G. Condorelli, A. Motta, I.L. Fragalà, J. Mater. Chem. 19 (2009) 3407.
[35] Domenico A. Cristaldi, Salvatrice Millesi, Placido Mineo, A. Gulino, J. Phys. Chem. C 117 (2013) 16213.
[36] M.H.V. Werts, R.T.F. Jukes, J.W. Verhoeven, Phys. Chem. Chem. Phys. 4 (2002) 1542.
[37] P.A. Joy, P.S.A. Kumar, S.K. Date, J. Phys. Condens. Matter 10 (1998) 11049.
[38] J.H. Van Vleck, Theory of Electric and Magnetic Susceptibilities, Oxford, Chapter IX, 1932.